Published OnlineFirst April 26, 2019; DOI: 10.1158/1535-7163.MCT-18-0804

Small Molecule Therapeutics

Molecular Cancer Therapeutics

Loss of Notch1 Activity Inhibits Prostate Cancer Growth and Metastasis and Sensitizes Prostate Cancer Cells to Antiandrogen Therapies

Meghan A. Rice, En-Chi Hsu, Merve Aslan, Ali Ghoochani, Austin Su, and Tanya Stoyanova

Abstract

Prostate cancer remains among the leading causes of cancer-related deaths in men. Patients with aggressive disease typically undergo hormone deprivation therapy. Although treatment is initially very successful, these men commonly progress to lethal, castration-resistant prostate cancer (CRPC) in 2 to 3 years. Standard therapies for CRPC include second-generation antiandrogens, which prolong patient lifespan by only several months. It is imperative to advance our understanding of the mechanisms leading to resistance to identify new therapies for aggressive prostate cancer. This study identifies Notch1 as a therapeutic target in prostate cancer. Loss of *NOTCH1* in aggressive prostate cancer cells decreases proliferation, invasion, and tumorsphere formation. Therapeutic inhibition of Notch1 activity with gamma secretase inhibitors RO4929097 or DAPT in prostate cancer cells further results in decreased proliferative abilities. Loss of *NOTCH1* and treatment of immunocompromised mice bearing prostate cancer xenografts with RO4929097 display significantly impaired tumor growth. Loss of *NOTCH1* additionally decreased metastatic potential of prostate cancer cells in invasion assays *in vitro* as well as *in vivo* experiments. Moreover, treatment with gamma secretase inhibitors or *NOTCH1* gene deletion synergized with antiandrogen therapies, enzalutamide or abiraterone, to decrease the growth of prostate cancer cells. Combination of gamma secretase inhibitors with abiraterone significantly inhibited cell migration and invasion, while combination with enzalutamide reversed enzalutamide-induced migration and invasion. These collective findings suggest loss of *NOTCH1* delays growth of CRPC and inhibits metastasis, and inhibition of Notch1 activation in conjunction with second-generation antiandrogen therapies could delay growth and progression of prostate cancer.

Introduction

Prostate cancer is the most common cancer affecting men, and the second leading cause of cancer-associated mortalities in men in the United States (1). Current treatments for aggressive prostate cancer, including androgen ablation therapy, have great short-term success yet frequently results in recurrence, at which point it is termed castration-resistant prostate cancer (CRPC; ref. 2). Treatment options include second-generation antiandrogens enzalutamide, abiraterone, or the recently FDA-approved apalutamide; chemotherapeutic agents docetaxel or cabazitaxel; or Provenge (Dendreon Pharmaceuticals LLC) prostate cancer immunotherapy (2–9). Ultimately due to the aggressive and highly metastatic nature of CRPC, patients often develop resistance to individual therapies, and to date, CRPC remains incurable. This highlights the urgent need to define new pathways that can drive the occurrence of advanced prostate cancer and evaluate novel therapies for advanced disease and metastatic CRPC.

Notch1 is a transmembrane glycoprotein belonging to the Notch family of receptors (Notch1/2/3/4). Involved in cell–cell signaling, Notch1 receptor is activated by ligands (Jagged 1/2 and Delta 1/3/4), initiating a multistep cleavage by members of the Disintegrin Metalloprotease (ADAM) families as well as the gamma secretase complex (10). This results in the cleavage of the intracellular domain of Notch1 (NICD1), which translocates to the nucleus (activated Notch1) as a transcriptional coactivator, regulating self-renewal, cell maintenance, and tumorigenesis (11–14). Alterations of the Notch1 receptor are found in many malignancies, acting in a context-dependent manner as either oncogenes or tumor suppressors (15).

In prostate cancer, while no genetic alterations of *NOTCH1* have been described, downregulation of Notch1 and its ligand Jagged1 decrease cell invasion, growth, and migration (16–18). Notch1 expression promotes epithelial-to-mesenchymal transition (EMT), seminal vesicle transformation, and metastatic occurrence (18–20). Furthermore, we previously demonstrated that Notch1 plays an important oncogenic role in the development of CRPC (21). We identified increased nuclear-activated NICD1 levels in high-risk prostate cancer and CRPC patient specimens over benign and low-risk disease, and determined NICD1 acts a driver for aggressive prostate adenocarcinoma and metastatic CRPC in conjunction with other common alterations observed in prostate cancer (Myc overexpression, loss of *PTEN*, or activation of the Ras signaling pathway; ref. 21). These findings indicate Notch1 is involved in the progression of prostate cancer and

Department of Radiology, Canary Center at Stanford for Cancer Early Detection, Stanford University, Palo Alto, California.

Note: Supplementary data for this article are available at Molecular Cancer Therapeutics Online (http://mct.aacrjournals.org/).

Corresponding Author: Tanya Stoyanova, Stanford University, 3155 Porter Drive, Palo Alto, CA 94304. Phone: 650-498-9331; Fax: 650-721-6921; E-mail: stanya@stanford.edu

Mol Cancer Ther 2019;18:1230–42

doi: 10.1158/1535-7163.MCT-18-0804

Published OnlineFirst April 26, 2019; DOI: 10.1158/1535-7163.MCT-18-0804

targeting Notch1 signaling may represent an effective therapy for aggressive disease (21).

Multiple strategies to inhibit the Notch pathway have been generated including targeting the activation of Notch receptors via gamma secretase inhibition (GSI; refs. 22–26). In preclinical studies of epithelial cancers, GSIs as single agents have demonstrated promising antitumorigenic abilities, as was the case for one of the GSIs described in this study, RO4929097 (27). Using two GSIs, RO4929097 and DAPT as well as loss of *NOTCH1* via CRISPR-Cas9 deletion, we aimed to determine the potential for loss of *NOTCH1* as a strategy to inhibit the growth of aggressive prostate cancer, metastasis, as well as Notch1 inhibition synergy with antiandrogen therapies.

Materials and Methods

Cell lines and culture

22RV1 cells were obtained from ATCC and C4-2 cells were a gift from Dr. Owen Witte's laboratory at UCLA (Los Angeles, CA). 22RV1 Delta-Notch1 cells were generated using CRISPR-Cas9 knockout of *NOTCH1* as described previously (21). 22RV1-Luc and 22RV1 Delta-Notch1-Luc cells were generated with lentiviral transduction of pHIV-Luc-ZsGreen, a kind gift from Bryan Welm (University of Utah, Salt Lake City, UT; Addgene plasmid #39196; http://n2t.net/addgene:39196; RRID: Addgene_39196). All cell lines are annually authenticated, most recently, through the Stanford Functional Genomics Facility. Cells were tested for the presence of *Mycoplasma* biannually using the Lonza Mycoalert Detection Kit (Lonza). Cells were cultured in RPMI supplemented with 10% FBS, 1% penicillin/streptomycin, and 1% L-Glutamine, with warmed Trypsin/EDTA (0.25%) used for dissociation. Cells were incubated at 37°C with 5% CO_2.

Colony formation assay

A total of 5×10^2 22RV1, C4-2, or 22RV1 Delta-Notch1 cells were plated per well of a 6-well plate in triplicate. Cells were treated with DMSO vehicle control, enzalutamide (5 μmol/L), abiraterone (5 μmol/L), DAPT (50 μmol/L), or RO4929097 (20 μmol/L; all compounds were purchased from Selleckchem, catalog numbers S1250, S2246, S2215, and S1575, respectively; refs. 28–30, 27). Cells were cultured for 9 days, with media and compounds changed every third day. Colonies were then fixed with methanol and stained with 0.1% crystal violet for 1 hour at room temperature. Plates were washed by submerging in a water bath for 1 hour. Colonies were counted, and colony formation rate determined (percentage), quantified as number of colonies per 5×10^2 cells × 100, as described previously (21).

Tumorsphere formation assay

A total of 1×10^4 22RV1 or Delta-Notch1 cells were plated in 50% Matrigel (Corning Inc), 50% supplemented RPMI in individual wells of a 24-well plate in triplicate. Cells were grown 15 days with media changed every third day. Wells were imaged on Leica stereomicroscope. 20× images were acquired per well in four quadrants and tumorsphere number per field was quantified, including any growth larger than 100 μm largest diameter, as measured in FIJI (31).

Cell viability assay

A total of 1×10^4 22RV1 or C4-2 cells were plated per well in a 96-well plate overnight. The next day, media were changed to 100 μL of media containing the indicated concentrations of drugs. Seventy-two hours later, 100 μL fresh media were added + 20 μL Cell-Titer Blue viability reagent (Promega), and plate with reagent was incubated 2 hours at 37°C prior to reading fluorescence on Tecan plate reader. Relative fluorescence units (RFUs) were graphed as fold change over vehicle control.

Cell invasion assay

22RV1, Delta-Notch1, or C4-2 cells were serum starved overnight in RPMI. Cells were then trypsinized, counted, and 5×10^4 were plated on top of Matrigel-coated Costar Transwell (Sigma-Aldrich) invasion chambers that were preincubated with serum-free RPMI. The bottom chamber was filled with RPMI supplemented with 10% FBS as a chemoattractant. In the case of drug-treated conditions, cells were pretreated for 72 hours prior to plating chambers, and both supplemented and unsupplemented media were treated with appropriate inhibitors to maintain treatment conditions. Chambers were incubated 24 hours for C4-2 cells or 36 hours for 22RV1 and Delta-Notch1, and then fixed with ice-cold methanol. Noninvading cells were removed from top of chamber with cotton swab, and then chambers were stained with 0.1% crystal violet for 1 hour. Chambers were washed in water, air dried overnight, and then imaged under Leica stereomicroscope at 161×. Five representative images were taken per chamber (three chambers per condition), and then cells were counted in each image and averaged. Experiments were performed in triplicate and analyzed using a Student *t* test.

Matrigel dot assay

A total of 2×10^5 C4-2 cells were resuspended in 20 μL Matrigel and gently pipetted into empty well of a 12-well plate, forming 3D dots. The dots were placed in incubator at 37°C for 20 minutes to solidify Matrigel. Media supplemented with inhibitors at aforementioned concentrations were then added, and subsequently changed every other day. Matrigel dots were imaged on day 0 at 20× for whole dot and 80×, measuring the leading edge of the dot in four quadrants. At 5 days after plating, dots were again imaged at the leading edge in the same locations. Images were overlaid, and distance migrated was measured using FIJI. Each treatment condition was performed in triplicate. For each dot, the average of all measurements was calculated. Triplicates for each condition were then averaged and SD was quantified. Student *t* test was used for analysis. Representative images are shown. Dots were then fixed with 2% paraformaldehyde in PBS for 10 minutes at room temperature. Wells were washed 3 × 5 minutes in PBS, and permeabilized 5 minutes with 0.1% Triton-X100. β-Actin (Santa Cruz Biotechnology, sc-47778) was used to stain the dots overnight, followed by Alexa Fluor 594 (Abcam), and counterstained with DAPI. Dots were reimaged at 100×.

Immunoblotting

Cells were harvested by scraping in PBS and lysed with RIPA lysis buffer containing protease and phosphatase inhibitors (Thermo Fisher Scientific). Tumor tissues were snap frozen in liquid nitrogen at time of harvest. Tissue was later homogenized in RIPA and sonicated. BCA assay was used to quantify protein, and then the samples diluted in 4× Laemmli buffer and boiled. Samples were run on Novex Tris-Glycine gels (Invitrogen), blocked for 1 hour in milk, and incubated in primary antibodies overnight in Tris-buffered saline containing 0.1% Tween-20. Secondary antibodies were applied for 1 hour after washing, and

Published OnlineFirst April 26, 2019; DOI: 10.1158/1535-7163.MCT-18-0804

then Pierce ECL Western Blotting Substrate (Thermo Fisher Scientific) was used to develop chemiluminescent signals on IVIS Lumina imager, with Living Image Software. Antibodies include anti-GAPDH sc-47724 (Santa Cruz Biotechnology); anti-Notch1 D1E11 #3608, anti-Cleaved Notch1 (Val1744) D3B8 #4147, (Cell Signaling Technology); anti-AR N-20, anti-Notch3 (Abcam), and secondary HRP-conjugated mouse and rabbit antibodies (Santa Cruz Biotechnology).

Animals. In conducting research using animals, the investigators adhere to the laws of the United States and regulations of the Department of Agriculture. Furthermore, all animal studies and procedures have been approved and performed in accordance with Stanford Administrative Panel on Laboratory Animal Care (APLAC), IACUC, as well as the USAMRMC Animal Care and Use Review Office (ACURO). NSG (NOD-SCID-IL2Rγ–null) mice (Jackson Laboratory), 6–8 weeks old, were used for all experiments, and housed at Stanford University animal facilities. The length (L), width (W), and height (H) of tumors as well as animal weights were measured every third day for subcutaneous tumors. Tumor volume was calculated by $(L \times W \times H)/2$.

GSI tumor treatment

Mice were castrated one week prior to cell implantation. 22RV1 or C4-2 cells (5×10^5) were injected subcutaneously (s.c.) into the flank in Matrigel. When tumors reached palpable size (50 mm^3 on average), animals were randomly assigned to treatment with vehicle (control) or with RO4929097 (10 mg/kg), purchased from Selleckchem. Vehicle and RO4929097 were dissolved in 2% DMSO + 30% PEG 300 + 5% Tween + ddH_20 and administered by oral gavage daily. Tumors graphed as fold change over the first measurable tumor volume of each tumor.

Delta-Notch1 tumors

Mice were castrated one week prior to cell implantation. A total of 5×10^5 22RV1 ($n = 10$) or Delta-Notch1 ($n = 9$ due to one tumor not grafting) cells were injected subcutaneously into the flank in Matrigel. Measurements began 3 days after implantation. Tumors were graphed as fold change.

Intracardiac metastasis model

A total of 1×10^5 22RV1-Luc or Delta-Notch1-Luc cells were injected into the left ventricle of the heart under isoflurane anesthesia. Bioluminescence signal in animals was imaged at 1 hour following injection procedure to ensure proper flow of cells into circulation, then at 7 and 14 days postprocedure.

Bioluminescent imaging

Mice were injected subcutaneously with 150 mg/kg D-Luciferin (Perkin Elmer) in 1× PBS, and placed into isoflurane anesthesia chamber. Five minutes postinjection, animals were transferred to Lago for bioluminescent imaging (Spectral Instruments Imaging) at Stanford Preclinical Imaging Facility at Porter Drive. Aura software was used for image acquisition and analysis. Briefly, animals were imaged 4 minutes at high binning. At time of sacrifice, animals were injected with Luciferin, euthanized, and then the organs were excised and *ex vivo* imaging was performed on tissues, placed in a petri dish, in a solution of 300 μg/mL D-Luciferin and imaged on IVIS Lumina imager.

Histology

At time of harvest, tumor or organ tissues were fixed in 10% formalin overnight at 4°C. Tissue was then transferred to 70% ethanol, processed into paraffin, and embedded. Formalin-fixed paraffin embedded (FFPE) tissue was sliced 4-μm–thick and attached to charged glass slides. Slides were heated to 65°C for 1 hour prior to deparaffinization, followed by hydration. Antigen retrieval was performed using a steamer, with 10 mmol/L sodium citrate buffer pH 6.0, or 1 mmol/L EDTA pH 8.0 (for Cleaved Notch1 Val1744 antibody only). After washing, 0.3% hydrogen peroxide solution was applied to slides to inactivate endogenous peroxidases, and then the slides were blocked in 2.5% horse (rabbit antibodies) or goat serum (mouse antibodies) (Vector Laboratories) for 1 hour at room temperature. Antibodies were applied in corresponding serum overnight at 4°C in a humidified chamber. The next day, after washing, secondary mouse or rabbit HRP (Vector Laboratories) was then applied for 1 hour. DAB (Dako Laboratories/Agilent) was used to stain the tissue, followed by counterstain in hematoxylin, and subsequent dehydration. Slides were cover-slipped in Faramount (Dako). Imaging was performed on Hamamatsu nanozoomer and photos were taken at 40× magnification. Anti-Cleaved Notch1, anti-E-Cadherin #3195, anti-Vimentin #5741 (Cell Signaling Technology); anti-Hes1, anti-Ki67, anti-Ku70 (Santa Cruz Biotechnology) were used for IHC.

Results

Loss of *NOTCH1* impairs CRPC cellular proliferation and invasion

On the basis of our previous studies and others implicating Notch1 in prostate cancer progression, invasion, metastasis, and CRPC development, we posited that inhibition of Notch1 would impair prostate cancer cell growth. Two GSIs, RO4929097 and DAPT, were tested for their ability to decrease activated Notch1 levels in C4-2 and 22RV1 CRPC cells, as well as our previously described 22RV1 CRISPR-Cas9 *NOTCH1* Knockout cells (Delta-Notch1; ref. 21). C4-2 and 22RV1 express high endogenous Notch1 and abundant activated or cleaved NICD1 (NICD1 Val1744; Fig. 1A; Supplementary Fig. S1A). GSI treatment of 22RV1 and C4-2 cells abolished activated NICD1 levels by 24-hour treatment, and was observed through 72 hours, while the two tested GSIs had no effect on NICD3 previously implicated in prostate cancer (Fig. 1B; Supplementary Fig. S1B).

Extended treatment with either GSI in 22RV1 and C4-2 cells decreased the colony-forming abilities of both CRPC lines (Fig. 1C), as well as their ability to form tumorspheres (Fig. 1D).

To eliminate concern of off-target effects of GSIs, experiments were performed with Delta-Notch1 cells compared against 22RV1 parental cells. Loss of *NOTCH1* decreased colony formation over parental 22RV1 cells (Fig. 2A). Treatment of Delta-Notch1 cells with either RO4929097 or DAPT had no effect on colony formation, suggesting the observed effects from GSI treatment appear to be dependent on Notch1 expression (Fig. 2B). Loss of *NOTCH1* was additionally responsible for decreased tumorsphere formation (Fig. 2C) of 22RV1 cells. Delta-Notch1 tumorsphere numbers were not affected by the addition of either RO4929097 or DAPT (Fig. 2D). These data indicate NICD1 expression to be important for CRPC cellular proliferation, and enforce the specificity of the Delta-Notch1 knockout cells.

Published OnlineFirst April 26, 2019; DOI: 10.1158/1535-7163.MCT-18-0804

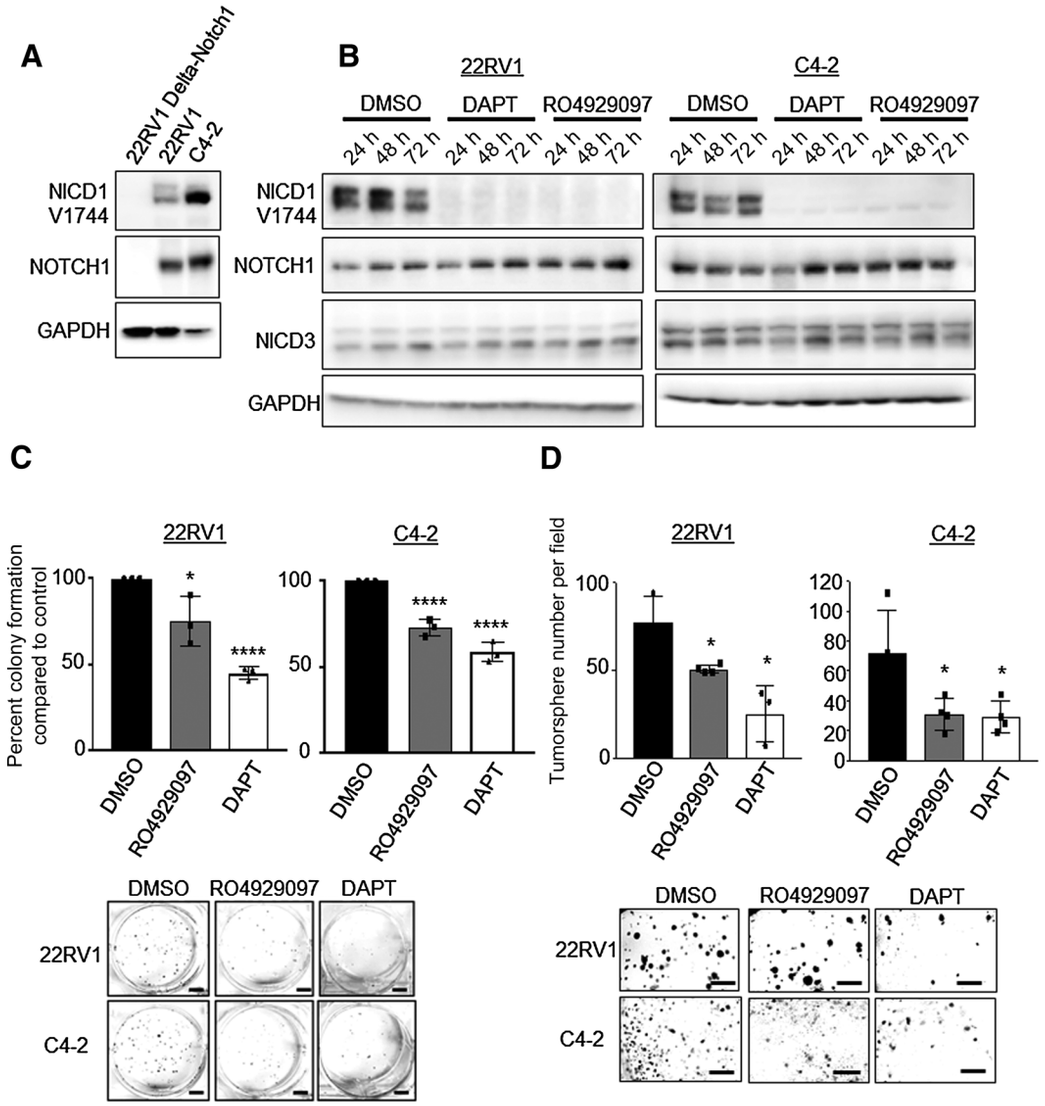

Figure 1.

GSI as a single therapeutic agent in prostate cancer cells impairs colony and tumorsphere formation. **A,** Immunoblot of human prostate cancer cells: 22RV1, C4-2, and 22RV1 *NOTCH1* knockout, Delta-Notch1. **B,** Immunoblot of time-course GSI treatment in 22RV1 or C4-2 prostate cancer cells. Cells were treated 24, 48, or 72 hours with inhibitors DAPT (50 μmol/L) or RO4929097 (20 μmol/L). Staining was performed for activated NICD1 (NICD1 Val1744), Notch1, NICD3, and GAPDH. **C,** Colony formation assay: 500 cells were plated per well in 6-well dish in triplicate. Cells were grown 9 days, with media and drugs changed every third day. Colonies were then fixed with methanol and stained with 0.1% crystal violet. Colonies were hand counted and graphed as percent colony formation over control treatment. Control treatment (DMSO) was normalized to 100%. Scale bar, 100 mm. Experiment is representative of three, performed in triplicate. **D,** Tumorsphere formation assay was performed with 1×10^4 22RV1 or C4-2 cells plated in 50% Matrigel in 24-well plate. Cells were treated with DAPT or RO4929097, and then grown for 15 days with media and inhibitors changed every third day. Scale bar, 250 mm. Error bars are ± SD. Using two-tailed Student *t* test: *, $P < 0.05$; ****, $P < 0.001$.

Loss of *NOTCH1* by gene deletion or therapeutic inhibition impairs CRPC tumor growth

To determine the effects of GSIs *in vivo*, subcutaneous 22RV1 or C4-2 xenografts were implanted in castrated NSG mice to mimic androgen ablation *in vivo*. RO4929097 (10 mg/kg) or vehicle control was administered via daily oral gavage. Fold change in tumor volume growth was markedly reduced in RO4929097 animals (Fig. 3A) with no observed toxicity (Supplementary Fig. S2). Notch1, cleaved Notch1 (NICD1 Val1744) and androgen receptor (AR) expression were confirmed by immunoblotting (Fig. 3B). Interestingly, there was a decrease in AR in C4-2 cells known to express full-length AR, which was not observed in 22RV1 expressing AR and AR-V7 (Fig. 3A and B; Supplementary Fig. S3). The mechanism through which inhibition of Notch activation regulates AR remains to be determined. Next, 22RV1 or Delta-Notch1 cells were implanted into castrated NSG mice. Delta-Notch1 tumors immediately displayed delayed growth, continued until time of sacrifice—30 days postimplantation when compared with the control animal tumor volume (Fig. 3C). As expected, Notch1 and NICD1 expression were

Published OnlineFirst April 26, 2019; DOI: 10.1158/1535-7163.MCT-18-0804

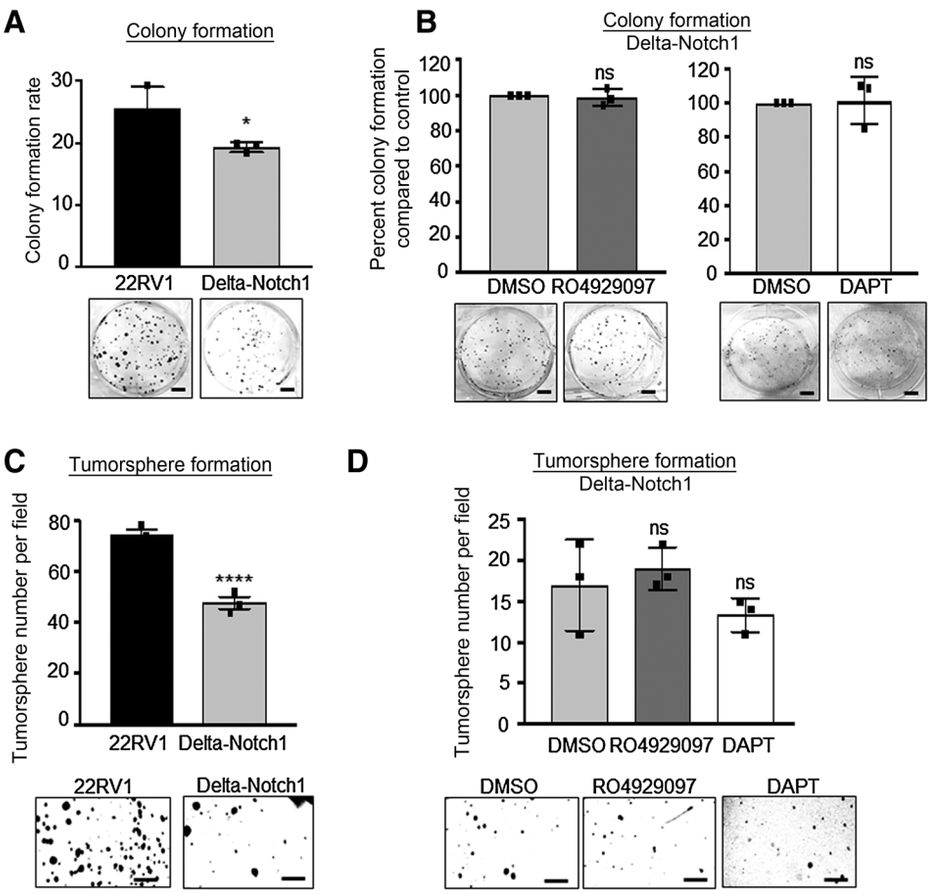

Figure 2.

Loss of Notch1 inhibits prostate cancer cell proliferation and tumorsphere formation. *In vitro* assays were performed on 22RV1 and Delta-Notch1 cells. **A** and **B,** Colony formation assay: 5×10^2 cells were plated per well in 6-well dish. Cells were grown 9 days with media changed every third day. Colonies were then fixed with methanol and stained with 0.1% crystal violet. Colonies were hand counted and graphed as colony formation rate (**A**) for 22RV1 and Delta-Notch1 cells, or percent colony formation compared with vehicle control (DMSO, normalized to 100%) for treated Delta-Notch1 cells (**B**). Delta-Notch1 cells were vehicle treated, RO4929097 treated (20 μmol/L), or DAPT treated (50 μmol/L). Scale bars, 100 mm. Tumorsphere formation assay: 1×10^4 22RV1 and Delta-Notch1 cells (**C**), or Delta-Notch1 cells treated with vehicle, RO4929097 (20 μmol/L), or DAPT (50 μmol/L; **D**) were plated in 50% Matrigel with RPMI in a 24-well plate. Cells were grown 15 days with media changed every third day. Scale bar, 250 mm. Experiments performed in triplicate with representative experiments shown. Using two-tailed Student *t* test: *, $P < 0.05$; ****, $P < 0.001$; ns, no significance. Error bars are ± SD.

undetectable in Delta-Notch1 tumors (Fig. 3D). Immunoblots were quantified in Supplementary Fig. S3. Histologic analysis of all tissues demonstrated reduction or loss of NICD1 in all treatment groups (Fig. 3E). This corresponded to a decrease of common Notch1 target gene, *HES1*. Proliferation was reduced in RO4929097 treatment as evidenced by Ki67 staining. We further noted substantial reversal of EMT markers upon loss of Notch1 or treatment with R04929097 observed via increased E-Cadherin corresponding to decreased Vimentin in all treatment groups (Fig. 3E). These experiments demonstrate that Notch1 may potentially represent a therapeutic target for CRPC.

Loss of *NOTCH1* decreases metastatic potential of CRPC

CRPC is highly metastatic in patients, with metastases most commonly occurring in bone, and secondarily in soft tissues, such as liver (32). We first tested whether loss of *NOTCH1* or therapeutic inhibition with GSIs would decrease CRPC cells' invasive behavior *in vitro*. Inhibition of Notch1 through treatment with DAPT (50 μmol/L) or RO4929097 (20 μmol/L) significantly impaired invasion in 22RV1 and C4-2 cells (Fig. 4A). Similar effect was observed in Delta-Notch1 cells (Fig. 4B).

Preclinical models of prostate cancer often struggle to recapitulate the human metastatic phenomenon of bone metastasis. However, 22RV1 cells implanted through intracardiac injection do commonly colonize in the hind limb of NSG mice as well as soft tissue (33). Using this model, we implanted 22RV1-Luc or Delta-Notch1-Luc cells via intracardiac injection to determine whether loss of *NOTCH1* impairs metastasis (Fig. 4C–I). Two weeks after implantation, Delta-Notch1-Luc animals had markedly lower detectable bioluminescence than their 22RV1-Luc counterparts, indicative of significantly reduced metastasis (Fig. 4C) and quantified as photons/second (Fig. 4D). The next day, mice were sacrificed and *ex vivo* imaging was performed on the mice, 5 minutes post luciferin injection (Fig. 4E). Organs imaged included liver, kidneys, heart, lungs, prostate, seminal vesicles, bladder, and hind limbs, and the remainder of the animal was imaged to ensure no bioluminescent signal remained (Fig. 4E). Strikingly, Delta-Notch1-Luc cells only colonized the mouse liver (6/6 animals), while the 22RV1-Luc group presented metastases in the liver (6/6), kidney (6/6), seminal vesicles (4/6), bone (3/6), and testes (3/6) (Fig. 4E).

Average liver bioluminescence was quantified and compared between the two groups after subtracting the background signal of a negative control (uninjected) animal from each liver signal (Fig. 4F). As apparent in whole-body images and liver sections, liver colonization was drastically impaired by the loss of *NOTCH1* (Fig. 4F–H). Representative liver bioluminescence is depicted in Fig. 4G. Bone samples were also collected (representative luminescent images in Fig. 4I). Liver samples (FFPE) were used to perform histologic comparisons between 22RV1-Luc, Delta-Notch1-Luc, and a negative uninjected control. Human Ku70, a protein involved with nonhomologous end-joining and the repair of DNA double-strand breaks, was used as proxy for human-specific staining of 22RV1-Luc and Delta-Notch1-Luc

Published OnlineFirst April 26, 2019; DOI: 10.1158/1535-7163.MCT-18-0804

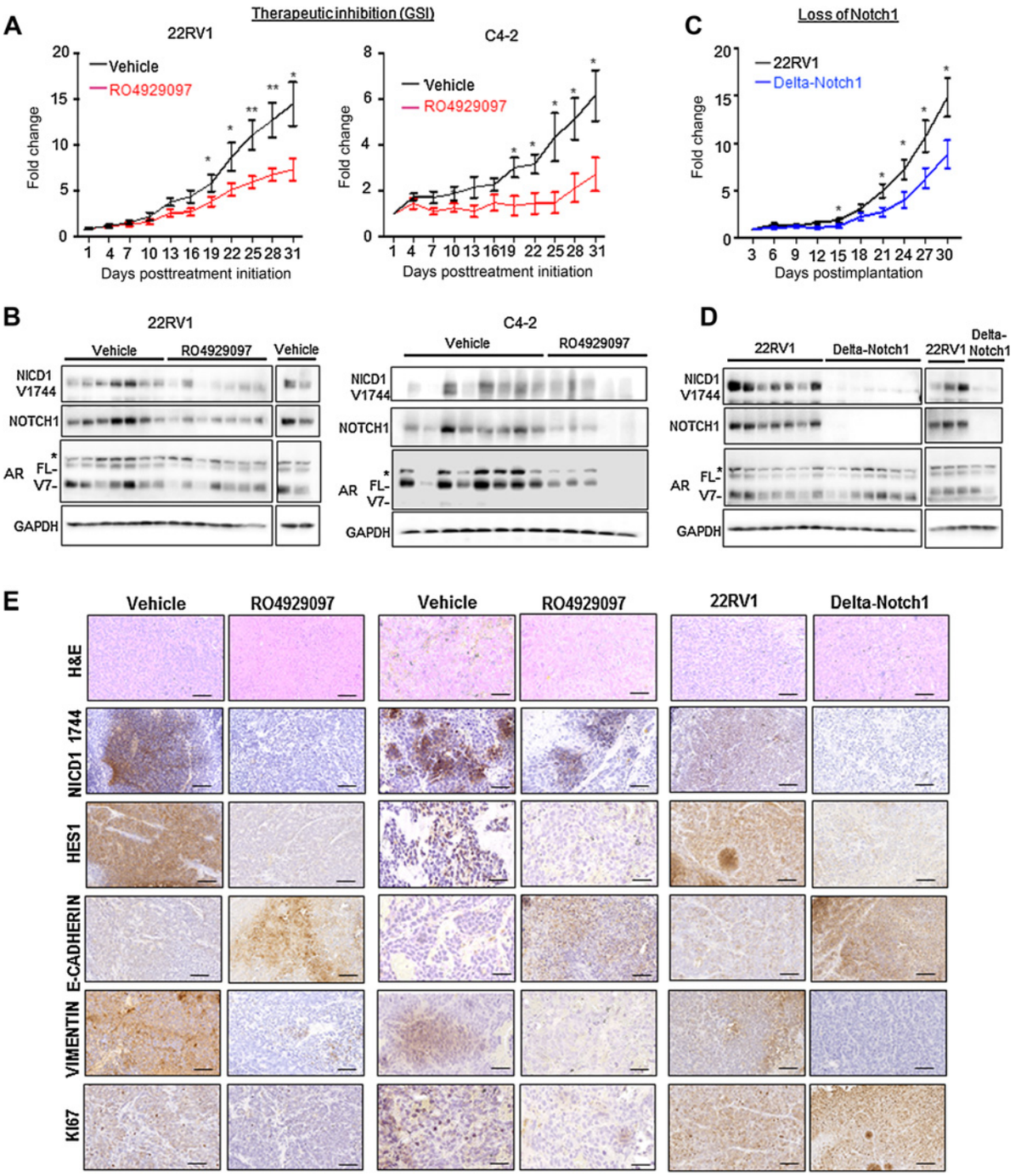

Figure 3.

Therapeutic inhibition of Notch1 impairs tumor formation of CRPC. **A,** A total of 5×10^5 22RV1 or C4-2 cells were implanted subcutaneously into castrated NSG mice (22RV1 $n = 9$ Vehicle; 22RV1 $n = 7$ RO4929097; C4-2 $n = 11$ Vehicle; C4-2 $n = 10$ RO4929097). Tumors were grown to palpable size (50 mm^3) and randomly distributed. At 50 mm^3, treatment was initiated (plotted as day 1). Animals were gavaged daily at 10 mg/kg of RO4929097 or vehicle control. **B,** Immunoblot analysis of 22RV1, or C4-2 tumor tissue for NICD1 V1744, Notch1, AR, and GAPDH. **C,** A total of 5×10^5 22RV1 or Delta-Notch1 cells were implanted subcutaneously into castrated NSG mice ($n = 10$). Tumor height (h), width (w), and length (l) were measured every third day and tumor volumes calculated as: $(h \times w \times l)/2$. Tumors graphed as fold change ± SEM, and analyzed for each time point by Student t test. *, $P < 0.05$; **, $P < 0.01$. **D,** Immunoblot analysis of 22RV1 or Delta-Notch1 tumor tissue for NICD1 V1744, Notch1, AR, and GAPDH. **E,** IHC of FFPE tumor tissue from 22RV1 and C4-2 xenografts treated with RO4929097 as well as Delta-Notch1 for NICD1 1744, Hes1, E-Cadherin, Vimentin, and Ki67, as well as histologic analysis with H&E. Images were taken at 40× and are representative of treatment group. Scale bars, 50 μm. *, a nonspecific band; FL, androgen receptor full length; V7, androgen receptor splice variant 7.

Published OnlineFirst April 26, 2019; DOI: 10.1158/1535-7163.MCT-18-0804

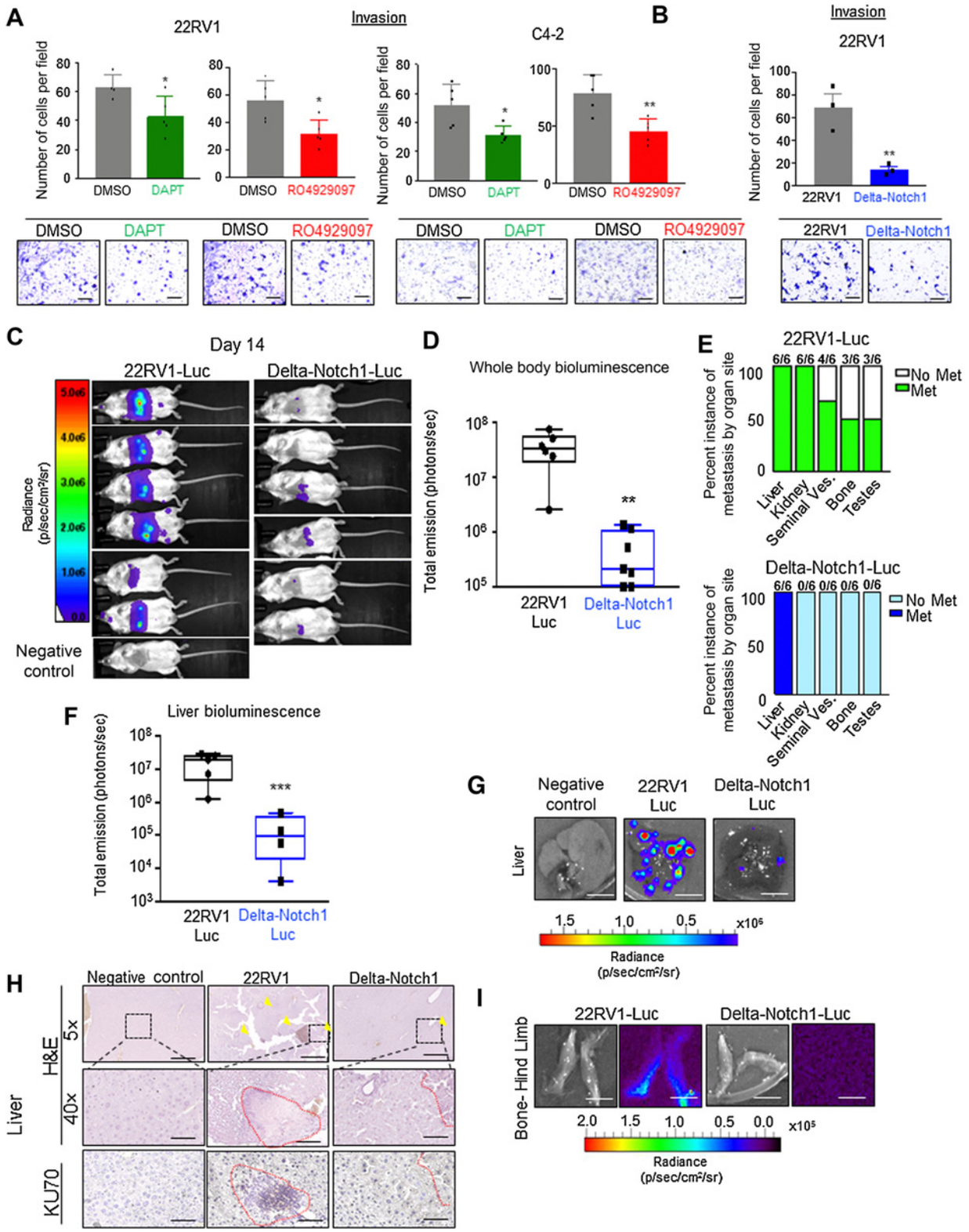

Published OnlineFirst April 26, 2019; DOI: 10.1158/1535-7163.MCT-18-0804

cells (Fig. 4H). We observed highly infiltrated livers in the 22RV1-Luc group depicted in histologic invasion of human epithelial cells into mouse livers, with significantly fewer observations in Delta-Notch1 tissue, consistent with bioluminescent findings (Fig. 4H). Collectively, these results demonstrate that loss of *NOTCH1* significantly impaired the metastatic potential of 22RV1 CRPC cells.

Notch1 inhibition synergizes with antiandrogens enzalutamide and abiraterone to inhibit prostate cancer cell proliferation *in vitro*

Inhibition of Notch receptor activation has demonstrated a unique ability to sensitize tumors to chemotherapies (34–36). We previously demonstrated expression of nuclear NICD1 in CRPC patient samples, reflecting Notch1 activation is significantly elevated in CRPC (21). To determine whether Notch1 inhibition could sensitize CRPC to second-generation antiandrogens, we utilized RO4929097 and DAPT to treat 22RV1 cells *in vitro* alone, or in conjunction with enzalutamide or abiraterone. Effects of combination therapy on cellular viability were modest suggesting low toxicity, with the greatest combined impact from abiraterone combined with either GSI (Supplementary Fig. S4).

Cells were then subjected to a colony formation assay with either RO4929097 or DAPT in combination with enzalutamide or abiraterone. As expected, treatment with enzalutamide as an independent drug in 22RV1 cells did not impact cell growth due to the known presence of androgen receptor splice variant 7 (AR-V7; Fig. 5A and B; Supplementary Fig. S5). In contrast to the short-term viability assay, GSI combination with enzalutamide synergized to decrease CRPC cell growth measured by colony formation (Fig. 5A and B). These effects were even more pronounced when performed with abiraterone (Fig. 5C and D; Supplementary Fig. S5).

To confirm the specificity of this effect to inhibition of Notch1, we performed the colony formation combination therapy experiments in Delta-Notch1 cells. Delta-Notch1 cells exhibited decreased colony formation potential compared with 22RV1 parental cells as previously observed, and further synergized with the addition of enzalutamide or abiraterone to impair proliferative colony formation (Fig. 5E; Supplementary Fig. S5).

Notch1 inhibition synergizes with antiandrogens enzalutamide and abiraterone to inhibit prostate cancer cell invasion and migration

As we have observed, loss of Notch1 leads to a significant decrease in the metastatic potential of CRPC *in vitro* and *in vivo*. We further assessed whether combinatorial treatment of GSIs with antiandrogen therapy would affect invasive potential of CRPC cells. We utilized two assays of cell motility. First, traditional Matrigel transwell assays were plated with 22RV1 or C4-2 cells pretreated for 72 hours with the same concentrations of DAPT, RO4929097, enzalutamide, abiraterone, or combination thereof as described above. At the time of plating for invasion, cells were counted again to ensure plating of equal number of cells. After 24-hour incubation for C4-2 cells and 36-hour incubation for 22RV1 cells, chambers were harvested, fixed, and stained with crystal violet. As we already established, DAPT and RO4929097 inhibited invasion in both 22RV1 and C4-2 cells. Enzalutamide, while an effective short-term therapeutic for patients with CRPC, was recently reported to increase CRPC invasiveness (37). Enzalutamide displayed a consistent increase in invasion in our assays (Fig. 6A and B). To this end, combination of enzalutamide with either GSI had invasion levels similar to that of DAPT or RO4929097 (Fig. 6A and B). This suggested that cotreatment with GSIs ablated the effects of enzalutamide-induced cellular invasion. Abiraterone had no effect on cellular invasive potential, and in combination, abiraterone with DAPT or RO4929097 synergized to significantly decrease invasion (Fig. 6A and B).

To further validate this phenotype, we performed a Matrigel Dot assay in which C4-2 cells were plated in 100% Matrigel as a 3D dot on a cell culture plate. These dots were treated with GSI and antiandrogen combination therapy for a total of 5 days. The dots were imaged at days 0 and 5 allowing us to measure the distance cells migrated outside of the Matrigel Dot. Results for C4-2 cell migration confirmed the observed invasion phenotype in that either DAPT or RO4929097 decreased cell migration (Fig. 6C and D; Supplementary Fig. S6). Furthermore, enzalutamide again increased cell migration ability, and GSIs were able to reverse and significantly decrease migratory ability of enzalutamide-treated cells (Fig. 6C; Supplementary Fig. S6A). While abiraterone had no effect on migration, abiraterone strongly synergized with GSIs to decrease migration (Fig. 6D; Supplementary Fig. S6B). This experiment was performed for 22RV1 cells as well but they did not escape the Matrigel capsule at the experimental time-point and thus migration measured by Matrigel Dot assay was not assessed in these cells (Supplementary Fig. S7).

Our study suggests that loss of *NOTCH1* through genetic deletion or therapeutic inhibition sensitized CRPC cells to antiandrogens to decrease cell growth and in the case of abiraterone, invasion and migration and inhibit enzalutamide-driven invasion and migration. While GSI in combination with enzalutamide

Figure 4.

Loss of Notch1 decreased metastatic potential of CRPC. **A,** 22RV1 or C4-2 cells were pretreated 72 hours with RO4929097 (20 μmol/L) or DAPT (50 μmol/L). Cells were serum starved overnight and 5×10^4 were plated in Matrigel invasion chambers and incubated 36 or 24 hours, respectively. Scale bars, 250 μm. **B,** 22RV1 or Delta-Notch1 cells were serum starved overnight, then 5×10^4 were plated in Matrigel transwell chambers. Chambers were incubated 36 hours, then fixed with methanol, and stained with crystal violet. For each condition, 5 fields were captured per chamber, number of cells per field were counted, then averaged for three chambers. Error bars, ± SD. Scale bars, 250 μm. **C,** A total of 1×10^5 22RV1-Luc or Delta-Notch1-Luc cells were injected intracardially into NSG mice. Animals were subjected to intraperitoneal (i.p.) injection with 150 mg/kg D-luciferin and imaged at 0 hours, 7 days, and 14 days. Final imaging at 14 days is pictured with all animals set to the same radiance scale. **D,** Quantification of whole-animal bioluminescence is plotted as total emission (photons/sec), representing each value in a box and whisker plot on Log_{10} scale. **E,** *Ex vivo* imaging was performed on all organs, with signal maintained in 300 μg/mL D-luciferin after harvest. Instance of organs with positive bioluminescence was graphed out of 6 animals. **F,** Liver bioluminescence was set to the same radiance scale for all animals, then quantified as radiance (p/sec/cm^2/sr) and graphed on Log_{10} scale in box and whisker plot. **G,** Representative bioluminescent images of liver from 22RV1-Luc, Delta-Notch1-Luc, or negative control (uninjected with cells) animals. Scale bar, 1 cm. **H,** Excised livers were fixed in formalin and paraffin embedded. Tissues were used to perform H&E (5× and 40×) as well as IHC for human KU70. Yellow arrowheads indicate visible metastatic lesions. Scale bars, 500 μm and 50 μm, respectively. **I,** Representative bioluminescent images of bone metastasis from 22RV1-Luc or Delta-Notch1 conditions. Scale bar, 1 cm; *, $P < 0.05$; **, $P < 0.01$; ***, $P < 0.005$.

Published OnlineFirst April 26, 2019; DOI: 10.1158/1535-7163.MCT-18-0804

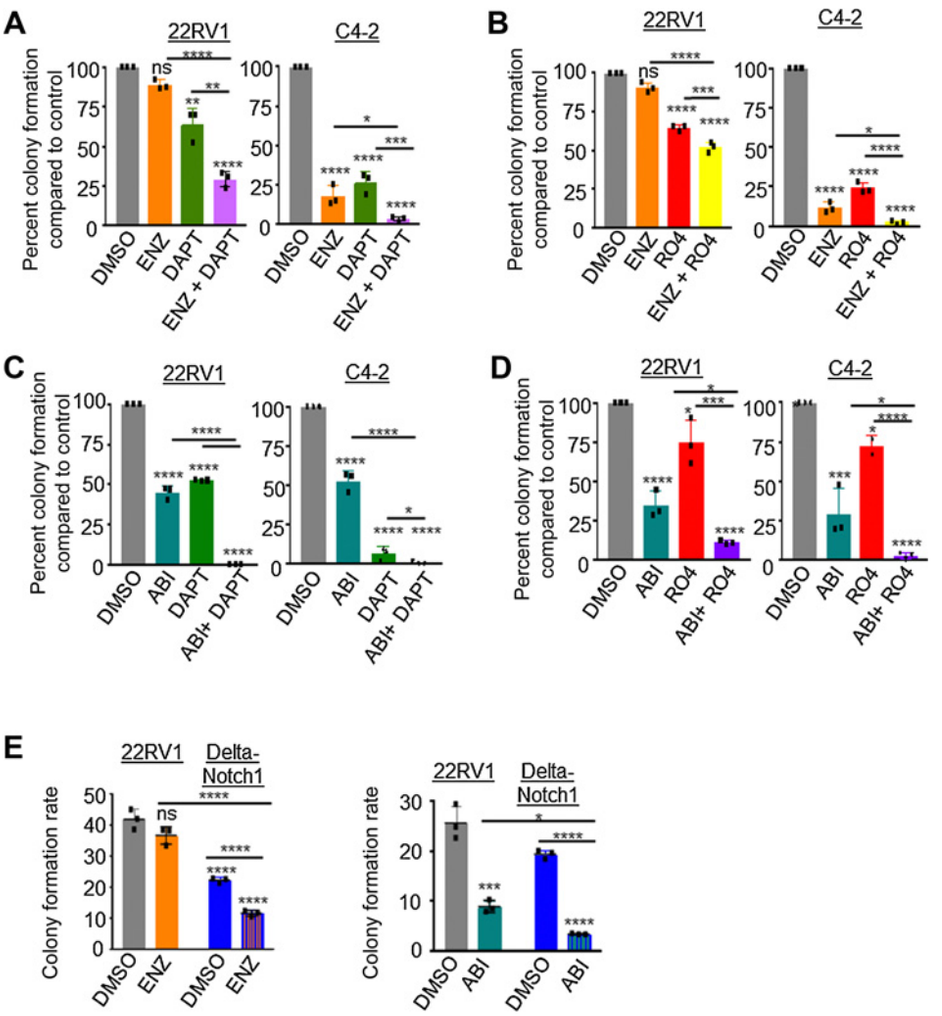

Figure 5.
Notch1 inhibition synergizes with antiandrogens enzalutamide and abiraterone to inhibit prostate cancer cell proliferation *in vitro*. **A,** Colony formation assay: 5×10^2 22RV1 or C4-2 cells were plated per well in 6-well dish, treated with vehicle (DMSO) control, enzalutamide (ENZ) 5 μmol/L; DAPT 50 μmol/L, enzalutamide + DAPT, or DMSO; ENZ; RO4929097 (RO4) 20 μmol/L; or enzalutamide + RO4 (**B**). Cells were grown 9 days, with media and drugs changed every third day. Colonies were then fixed with methanol and stained with 0.1% crystal violet. Control treatment (DMSO) was normalized to 100%. Colony formation assay was performed for DMSO control, abiraterone (ABI) 5 μmol/L, DAPT 50 μmol/L, abiraterone + DAPT (**C**) or DMSO, abiraterone, RO4929097 (RO4) 20 μmol/L, or ABI + RO4 (**D**). Colonies were hand counted and graphed as percent colony formation compared with control (vehicle). Control treatment (DMSO) was normalized to 100%. **E,** Colony formation of 22RV1 compared against Delta-Notch1 cells in the presence of enzalutamide, abiraterone, or DMSO control. Graphed as colony formation rate to compare across cell lines. All experiments performed in triplicate with representative images shown. *, $P < 0.05$; ***, $P < 0.005$; ****, $P < 0.001$; ns, no significance. Error bars ± SD.

is also a potent inhibitor of cell growth, these combinations play an additional role in reversing an enzalutamide-induced increase in invasive phenotype *in vitro*.

Discussion

A recent study corroborates our findings in which GSI inhibits oncogenic activity associated with prostate cancer cells (38). This study suggests the effect of GSI treatment on prostate cancer cells is due to inhibition of Notch3, based on an observation of upregulated *NOTCH3* mRNA in publicly available prostate cancer patient datasets. Our studies previously implicated Notch1 upregulation as a driver of prostate adenocarcinoma in conjunction with other alterations of prostate cancer, with increased Notch1 levels correlating with prostate cancer Gleason grade and CRPC (21). Herein, we inhibited Notch through GSI treatment as well as *NOTCH1* knockout, and observe comparable phenotypes of decreased oncogenesis, supporting Notch1 as a therapeutic target, but not Notch3.

Work by Mohamed and colleagues found GSI can synergize with enzalutamide, abiraterone, as well as another antiandrogen, bicalutamide to decrease cell proliferation, viability, and apoptosis of ERG-positive prostate cancer cells (VCaP), as Notch1 and 2 were found to be targets of ERG (39). ERG is an ETS family transcription factor commonly found increased in prostate cancer in roughly 50% of patients due to gene fusions with *TMPRSS2* serine protease (40). While this study suggests there is no impact of ERG-negative cells when GSI therapy is attempted, CRPC cell lines were not tested. 22RV1 and C4-2 are both ERG-negative CRPC cell lines. These cells being affected by *NOTCH1* loss or inhibition, paired with our previous work observing increased NICD1 in patient samples in progression to CRPC, reflect Notch1 signaling increases in CRPC, likely through an alternative ERG-independent mechanism.

In this article, we determined that loss of *NOTCH1* impaired *in vitro* invasion and *in vivo* metastatic colonization of 22RV1 cells. Our previous work determined that Notch1, when acting as a driver of prostate cancer progression to CRPC in combination with other known alterations in prostate cancer enriches for an epithelial-to-mesenchymal transition (EMT; ref. 21). Furthermore, overexpression of Notch1 increases invasion of prostate cancer cells (18). We verified this signature in Delta-Notch1 tumors as well as C4-2 or 22RV1 tumors treated with RO4929097. Not only were tumor volumes less with RO4929097 treatment or loss of Notch1, but upon analyzing the pathology of the tumors, we observed increases in epithelial marker E-Cadherin, as well as a

Published OnlineFirst April 26, 2019; DOI: 10.1158/1535-7163.MCT-18-0804

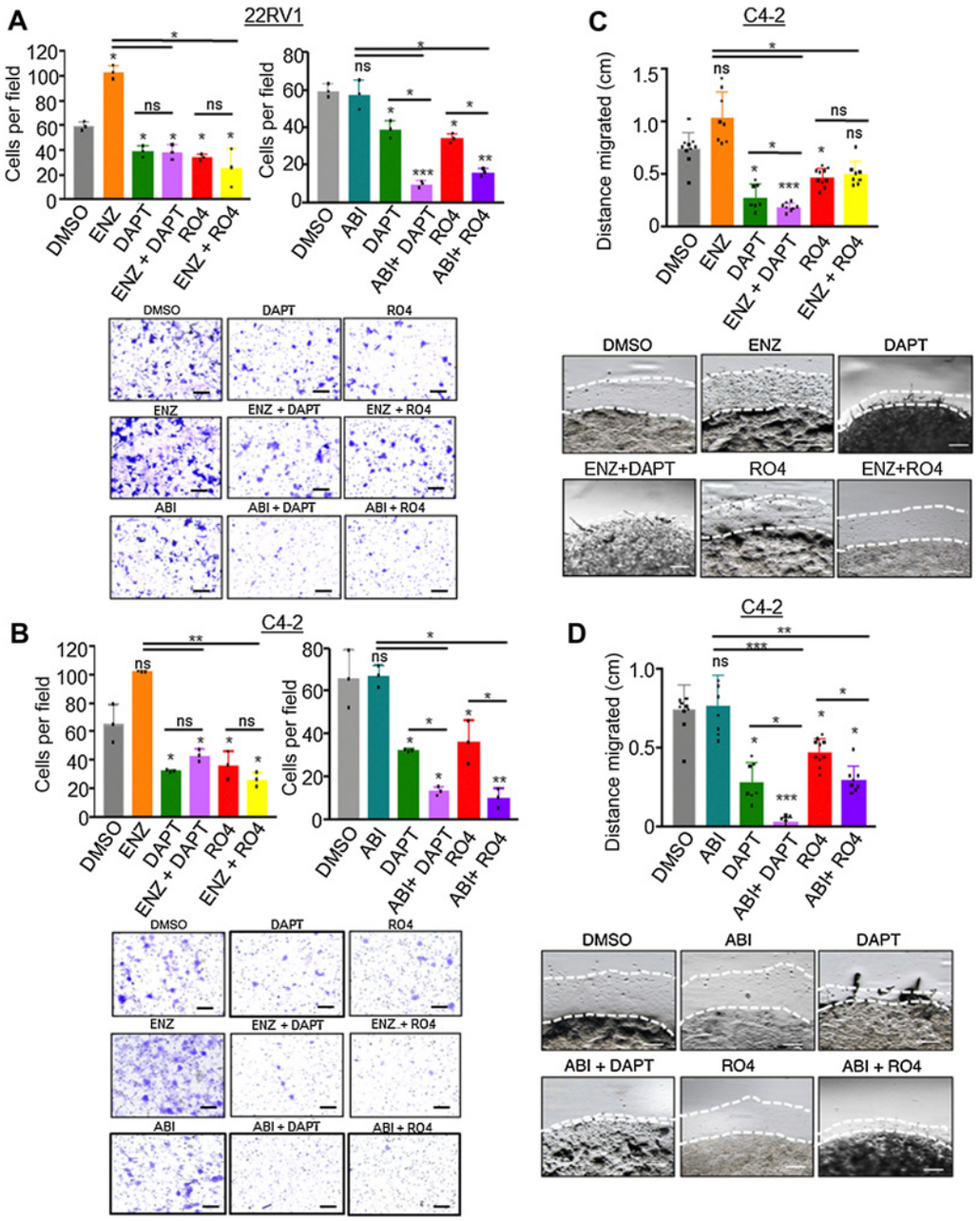

Figure 6.

Notch1 inhibition synergizes with antiandrogens enzalutamide (ENZ) and abiraterone (ABI) to inhibit prostate cancer cell invasion and migration *in vitro*. For invasion assays, 5×10^4 cells were plated in Matrigel-coated transwell invasion chambers. Cells were drug treated 72 hours prior to serum starving overnight, and plating in chambers. **A,** 22RV1 cells were treated with DAPT (50 μmol/L), enzalutamide (5 μmol/L), abiraterone (5 μmol/L), RO4929097 (RO4; 20 μmol/L), or combination of enzalutamide with DAPT or RO4 and abiraterone with DAPT or RO4. **B,** C4-2 cells were treated with DAPT (50 μmol/L), enzalutamide (5 μmol/L), abiraterone (5 μmol/L), RO4929097 (RO4; 20 μmol/L), or combination of enzalutamide with DAPT or RO4 and abiraterone with DAPT or RO4. Chambers were incubated 36 hours for 22RV1 and 24 hours for C4-2 cells, then fixed in methanol and stained in 0.1% crystal violet. Five images were captured per chamber at 161X, performed in triplicate chambers and averaged. Experiments were performed concurrently and graphed separately for each cell line for ease of visualization, thus DMSO, DAPT, and RO4 conditions are based on the same samples in these graphs. **C** and **D,** A total of 2×10^5 C4-2 cells were resuspended in 20 μL Matrigel and plated as a 3D dot on a 12-well plate. After Matrigel solidified, media were added and wells were treated with enzalutamide, DAPT, RO4, combined enzalutamide with DAPT or RO4 (**C**) or abiraterone, DAPT, RO4, or combined abiraterone with DAPT or RO4. Media were changed every 48 hours. Dots were imaged at four leading edges at days 0 and 5, and distance migrated (millimeters, mm) was calculated. Enzalutamide and abiraterone experiments were performed concurrently, then graphed separately for ease of visualization, thus in (**C**) and (**D**), DMSO, DAPT, and RO4 conditions are based on the same samples. Scale bars, 250 μm. All experiments performed in triplicate with representative images shown. *, $P < 0.05$; **, $P < 0.01$; ***, $P < 0.005$; ns, no significance; error bars, ± SD.

Published OnlineFirst April 26, 2019; DOI: 10.1158/1535-7163.MCT-18-0804

decrease of Vimentin, a mesenchymal cell marker, indicating an EMT reversal. This observation of Notch1 inhibition reversing EMT could attribute to the decreased invasive and metastatic properties we observed herein.

Loss of *NOTCH1* in this study synergized with abiraterone or enzalutamide to decrease prostate cancer growth and invasion. These antiandrogen therapies offered as treatment in patients with hormone-refractory prostate cancer often result in resistance. Several studies have determined that androgen deprivation therapies such as enzalutamide can themselves cause EMT and lead to resistance to enzalutamide therapy (37). Interestingly, cotreatment with GSI prevented the enzalutamide-induced increase of prostate cancer cell invasion, and in the case of abiraterone, synergize to decrease cellular invasion and migration. Notch1 and AR, both transcription factors, have no known direct interactions, or reported overlapping downstream targets in prostate cancer. One mechanism in which Notch1 and AR have cross-talk is hypoxia, involved in prostate cancer progression and is associated with hormone therapy resistance due to regulation of PSA and AR target genes (41). It has been previously reported that hypoxia requires Notch signaling to maintain undifferentiated cell states common to hypoxic environments (42). Therefore, it stands to reason that in hypoxic environments, Notch1 may be involved in hypoxia-associated androgen resistance. While transcription factor cross-talk among Notch1 and AR target genes could be involved, Notch receptors have been implicated in chemoresistance independent of AR. In these studies, it was shown that another GSI, PF-03084014 targets a well-known facet of Notch1 signaling, stem cells. Inhibition of prostate cancer stem cells with GSI was responsible for sensitizing chemoresistant cells to docetaxel (34, 36). These mechanisms should be explored to determine the full potential of Notch1-regulated hormone therapy resensitization. Another possibility is that Notch1 regulation of stem cell renewal is independent of AR. Zhang and colleagues demonstrated that introduction of NICD1 into AR-negative PC3 cells increased tumorsphere formation as well as cancer stem cell surface markers, contributing to self-renewal (18). In the prostate, Notch1 signaling can occur downstream of TGFβ, a well-known signal transduction pathway that maintains prostate stem cell quiescence (43). Together, Notch1 and TGFβ aid in maintaining prostate basal cell lineage, such that inhibition on Notch1 signaling may delay prostate cancer by delaying basal cell to luminal cell differentiation (43).

Although GSIs have been tested in clinical trials for epithelial cancers with promising results, they have not demonstrated durable antitumor effects as single agents (22). Despite common high toxicity issues surrounding GSIs, RO4929097 was safely administered to the animals in our preclinical studies, as well as in clinical trials coadministered with multiple cancer treatments (44–47). Combination therapy with GSI has shown promising partial responses in solid tumors, even sensitizing chemoresistant CRPC (34, 35). Several new strategies are being examined for clinical inhibition of Notch1. siRNAs for *NOTCH1* have shown promising *in vivo* results in models of prostate cancer, where siRNA was delivered to prostate-specific membrane antigen (PSMA)-positive prostate cancer cells, inducing apoptosis (48). *NOTCH1* siRNA therapy has additionally demonstrated oncogenic inhibition of *in vivo* models of gastric cancer and melanoma (49, 50). Likewise, mAbs specifically inhibiting Notch1 by targeting the negative regulatory region (NRR) of the Notch1 receptor have shown promising tumor growth inhibition in adenoid cystic carcinoma (ACC) and T-cell acute lymphoblastic leukemia (T-ALL) and some are undergoing clinical trials for treatment of solid tumors (25, 51–53).

Our study demonstrates the merit of further studying Notch1 inhibition as a treatment for CRPC as a single agent, as well as in combination with antiandrogen therapy. These treatments have the potential for delaying resistance to effective CRPC therapies, and resensitization of patients who are hormone refractory. It is likely that the benefit of Notch1-targeted therapies could extend to an even broader patient population, as *PTEN* loss, one of the most common genetic aberrations in prostate cancer, has been linked to Notch1 expression, and Notch1 inhibition has been demonstrated to synergize with antiandrogen therapies to induce apoptosis (39, 54). These findings in conjunction with our results demonstrate that Notch1 inhibition may represent a promising targeting strategy in a wide array of patients with prostate cancer.

Disclosure of Potential Conflicts of Interest

No potential conflicts of interest were disclosed.

Disclaimer

Opinions, interpretation, conclusions, and recommendations are those of the authors and not necessarily endorsed by the U.S. Army.

Authors' Contributions

Conception and design: M.A. Rice, T. Stoyanova
Development of methodology: M.A. Rice, E.-C. Hsu
Acquisition of data (provided animals, acquired and managed patients, provided facilities, etc.): M.A. Rice, E.-C. Hsu, A. Ghoochani, A. Su, T. Stoyanova
Analysis and interpretation of data (e.g., statistical analysis, biostatistics, computational analysis): M.A. Rice, T. Stoyanova
Writing, review, and/or revision of the manuscript: M.A. Rice, E.-C. Hsu, A. Ghoochani, A. Su, T. Stoyanova
Administrative, technical, or material support (i.e., reporting or organizing data, constructing databases): M.A. Rice, E.-C. Hsu, M. Aslan
Study supervision: T. Stoyanova

Acknowledgments

The authors would like to thank Dr. James Brooks and Dr. Donna Peehl for their thoughtful guidance and suggestions and the continued support of the Canary Foundation. T. Stoyanova is supported by the Canary Foundation, the NIH/NCI K99/R00 Pathway to Independence Award 4R00CA184397 and R03CA230819, the U.S. Army Medical Research Acquisition Activity through the Congressionally Directed Medical Research Program (CDMRP) under award no. W81XWH1810323, the McCormick and Gabilan Faculty Award. M.A. Rice is supported by the U.S. Army Medical Research Acquisition Activity, through the Congressionally Directed Medical Research Program (CDMRP) under Award no. W81XWH1810141.

The costs of publication of this article were defrayed in part by the payment of page charges. This article must therefore be hereby marked *advertisement* in accordance with 18 U.S.C. Section 1734 solely to indicate this fact.

Received July 19, 2018; revised October 29, 2018; accepted April 24, 2019; published first April 26, 2019.

References

1. Siegel RL, Miller KD, Jemal A. Cancer statistics, 2018. CA Cancer J Clin 2018;68:7–30.
2. Feldman B, Feldman D. The development of androgen-independent prostate cancer. Nat Rev 2001;1:34–45.

3. Smith MR, Saad F, Chowdhury S, Oudard S, Hadaschik BA, Graff JN, et al. Apalutamide treatment and metastasis-free survival in prostate cancer. N Engl J Med 2018;378:1408–18.
4. Scher HI, Fizazi K, Saad F, Taplin ME, Sternberg CB, Miller K, et al. Increased survival with enzalutamide in prostate cancer after chemotherapy. N Engl J Med 2012;367:1187–97.
5. Beer TM, Armstrong AJ, Ranthkopf DE, Loriot Y, Sternberg CN, Higano CS, et al. Enzalutamide in metastatic prostate cancer before chemotherapy. N Engl J Med 2014;371:424–33.
6. Hussain M, Fizazi K, Saad F, Rathenbord P, Shore N, Ferreira U, et al. Enzalutamide in men with nonmetastatic, castration-resistant prostate cancer. N Engl J Med 2018;378:2465–74.
7. de Bono JS, Logothetis CJ, Molina A, Fizazi K, North S, Chu L, et al. Abiraterone and increased survival in metastatic prostate cancer. N Engl J Med 2011;364:1995–2005.
8. Kantoff PW, Higano CS, Shore ND, Berger ER, Small EJ, Penson DF, et al. Sipuleucel-T immunotherapy for castration-resistant prostate cancer. N Engl J Med 2010;363:411–22.
9. Oudard S, Fizazi K, Sengelov L, Daugaard G, Saad F, Hansen S, et al. Cabazitaxel versus docetaxel as first-line therapy for patients with metastatic castration-resistant prostate cancer: a randomized phase III trial-FIRSTANA. J Clin Oncol 2017;35:3189–97.
10. Schroeter E, Kisslinger J, Kopan R. Notch-1 signalling requires ligand-induced proteolytic release of intracellular domain. Nature 1998;393: 382–6.
11. Artavanis-Tsakonas S, Rand MD, Lake RJ. Notch signaling: cell fate control and signal integration in development. Science 1999;284:770–6.
12. Struhl G, Adachi A. Nuclear access and action of Notch in vivo. Cell 1998; 93:649–60.
13. De Strooper B, Annaert W, Cupers P, Saftig P, Craessaerts K, Mumm JS, et al. A presenilin-1-dependent gamma-secretase-like protease mediates release of Notch intracellular domain. Nature 1999;398:512–22.
14. Jarriault S, Brou C, logeat F, Schroeter EH, Kopan R, Israel A. Signaling downstream of activated mammalian Notch. Nature 1995;37:355–8.
15. Ranganathan P, Weaver KL, Capobianco AJ. Notch signalling in solid tumours: a little bit of everything but not all the time. Nat Rev Cancer 2011;11:338–51.
16. Santagata S, Demichelis F, Riva A, Varambally S, Hofer MD, Kutok JL, et al. JAGGED1 expression is associated with prostate cancer metastasis and recurrence. Cancer Res 2004;64:6854–7.
17. Zhu H, Zhou X, Redfieid S, Lewin J, Miele L. Elevated Jagged-1 and Notch-1 expression in high grade and metastatic prostate cancers. Am J Transl Res 2013;5:368–78.
18. Zhang L, Sha J, Yang G, Huang X, Bo J, Huang Y. Activation of Notch pathway is linked with epithelial-mesenchymal transition in prostate cancer cells. Cell Cycle 2017;16:999–1007.
19. Kwon OJ, Zhang L, Wang J, Su Q, Feng Q, Zhang XH, et al. Notch promotes tumor metastasis in a prostate-specific Pten-null mouse model. J Clin Invest 2016;126:2626–41.
20. Deng G, Zheng X, Jiang P, Chen K, Wang X, Jiang K, et al. Notch1 suppresses prostate cancer cell invasion via the metastasis-associated 1-KiSS-1 metastasis-suppressor pathway. Oncol Lett 2017;14:4477–82.
21. Stoyanova T, Riedinger M, Lin S, Faltermeier CM, Smith BA, Zhang KX, et al. Activation of Notch1 synergizes with multiple pathways in promoting castration-resistant prostate cancer. Proc Natl Acad Sci U S A 2016;113: E6457–66.
22. Purow B. Notch inhibition as a promising new approach to cancer therapy. Adv Exp Med Biol 2012;727:305–19.
23. Takebe N, Nguyen D, Yang S. Targeting notch signaling pathway in cancer: clinical development advances and challenges. Pharmacol Ther 2014;141: 140–9.
24. Ridgway J, Zhang G, Wu Y, Stawicki S, Liang WC, Chanthery Y, et al. Inhibition of Dll4 signalling inhibits tumour growth by deregulating angiogenesis. Nature 2006;444:1083–7.
25. Wu Y, Cain-Hom C, Choy L, Hagenbeek TJ, de Leon GP, Chen Y, et al. Therapeutic antibody targeting of individual Notch receptors. Nature 2010;464:1052–7.
26. Moellering R, Cornejo M, Davis TN, Del Bianco C, Aster JC, Blacklow SC, et al. Direct inhibition of the NOTCH transcription factor complex. Nature 2009;462:182–8.
27. Luistro L, He W, Smith M, Packman K, Vilenchik M, Carvajal D, et al. Preclinical profile of a potent gamma-secretase inhibitor targeting notch signaling with in vivo efficacy and pharmacodynamic properties. Cancer Res 2009;69:7672–80.
28. Tran C, Ouk S, Clegg NJ, Chen Y, Watson PA, Arora V, et al. Development of a second-generation antiandrogen for treatment of advanced prostate cancer. Science 2009;324:787–90.
29. Pinto-Bazurco Mendieta MA, Megri M, Jagusch C, Muller-Vleira U, Lauterbach T, Hartmann RW. Synthesis, biological evaluation, and molecular modeling of abiraterone analogues: novel Cyp17 inhibitors for the treatment of prostate cancer. J Med Chem 2008;51:5009–18.
30. Dovey HF, John V, Anderson JP, Chen LZ, de Saint Andrieu P, Fang LY, et al. Functional gamma-secretase inhibitors reduce beta-amyloid peptide levels in brain. J Neurochem 2001;76:173–81.
31. Schindelin J, Arganda-Carreras I, Frise E, Kaynig V, Longair M, Pietzsch T, et al. Fiji: an open-source platform for biological-image analysis. Nat Methods 2012;9:676–82.
32. Halabi S, Kelly WK, Ma H, Zhou H, Solomon NC, Fizazi K, et al. Meta-analysis evaluating the impact of site of metastasis on overall survival in men with castration-resistant prostate cancer. J Clin Oncol 2016;34: 1652–9.
33. Drake JM, Gabriel CL, Henry MD. Assessing tumor growth and distribution in a model of prostate cancer metastasis using bioluminescence imaging. Clin Exp Metastasis 2015;22:674–84.
34. Cui D, Dai J, Keller JM, Mizokami A, Xia S, Keller ET. Notch pathway inhibition using PF03084014, a gamma-secretase inhibitor (GSI), enhances the anti-tumor effect of docetaxel in prostate cancer. Clin Cancer Res 2015;21:4619–29.
35. Wang W, Wang L, Mizokami A, Shi J, Zou C, Dai J, et al. Down-regulation of E-cadherin enhances prostate cancer chemoresistance via Notch signaling. Chin J Cancer 2017;36:35.
36. Domingo-Domenech J, Vidal SJ, Rodriguez-Bravo V, Castillo-Martin M, Quinn SA, Rodriguez-Barrueco R, et al. Suppression of acquired docetaxel resistance in prostate cancer through depletion of Notch- and hedgehog-dependent tumor-initiating cells. Cancer Cell 2012;22:373–88.
37. Chen J, Li L, Yang Z, Luo J, Yeh S, Chang C. Androgen-deprivation therapy with enzalutamide enhances prostate cancer metastasis via decreasing the EPHB6 suppressor expression. Cancer Lett 2017;408:155–63.
38. Cui J, Wanh Y, Dong B, Qin L, Wang C, Zhou P, et al. Pharmacological inhibition of the Notch pathway enhances the efficacy of androgen deprivation therapy for prostate cancer. Int J Cancer 2018;143:645–56.
39. Mohamed AA, Tan SH, Xavier CP, Huang W, Ravindranath L, Jamal M, et al. Synergistic activity with NOTCH inhibition and androgen ablation in ERG-positive prostate cancer cells. Mol Cancer Res 2017;15:1308–17.
40. Yoshimoto M, Joshua AM, Chilton-Macneill S, Bayani J, Selvarajah S, Evans AJ, et al. Three-color FISH analysis of TMPRSS2/ERG fusions in prostate cancer indicates that genomic microdeletion of chromosome 21 is associated with rearrangement. Neoplasia 2006;8:465–9.
41. Horii K, Suzuki Y, Kondo Y, Akimoto M, Nishimura T, Yamabe Y, et al. Androgen-dependent gene expression of prostate-specific antigen is enhanced synergistically by hypoxia in human prostate cancer cells. Mol Cancer Res 2007;5:383–91.
42. Gustafsson MV, Zheng X, Pereira T, Gradin K, Jin S, Lundkvist J, et al. Hypoxia requires notch signaling to maintain the undifferentiated cell state. Dev Cell 2005;9:617–28.
43. Valdez JM, Zhang L, Su Q, Dakhova O, Zhang Y, Shahi P, et al. Notch and TGFbeta form a reciprocal positive regulatory loop that suppresses murine prostate basal stem/progenitor cell activity. Cell Stem Cell 2012;11: 676–88.
44. Richter S, Bedard PL, Chen EX, Clarke BA, Tran B, Hotte SJ, et al. A phase I study of the oral gamma secretase inhibitor R04929097 in combination with gemcitabine in patients with advanced solid tumors. Invest New Drugs 2014;32:243–9.
45. LoConte NK, Razak AR, Ivy P, Tevaarwerk A, Leverence R, Kolesar J, et al. A multicenter phase 1 study of gamma -secretase inhibitor RO4929097 in combination with capecitabine in refractory solid tumors. Invest New Drugs 2015;33:169–76.
46. Sahebjam S, Bedard PL, Castonguay V, Chen Z, Reedjik M, Liu G, et al. A phase I study of the combination of ro4929097 and cediranib in patients with advanced solid tumours. Br J Cancer 2013;109:943–9.

Published OnlineFirst April 26, 2019; DOI: 10.1158/1535-7163.MCT-18-0804

47. Diaz-Padilla I Hirte H, Oza AM, Clarke BA, Cohen B, Reedjik M, Zhang T, et al. A phase Ib combination study of RO4929097, a gamma-secretase inhibitor, and temsirolimus in patients with advanced solid tumors. Invest New Drugs 2013;31:1182–91.
48. Su Y, Yu L, Liu N, Guo Z, Wang G, Zheng J, et al. PSMA specific single chain antibody-mediated targeted knockdown of Notch1 inhibits human prostate cancer cell proliferation and tumor growth. Cancer Lett 2013;338: 282–91.
49. Yang Z, Qi Y, Zhang J, Luo R, Kang S. Small interfering RNA (siRNA)-mediated knockdown of Notch1 suppresses tumor growth and enhances the effect of IL-2 immunotherapy in malignant melanoma. J BUON 2015; 20:1553–64.
50. Zhao EH, Jin X, Shen ZY, Liu H, Cao H. Influence of silencing Notch1 on proliferation, migration and invasion of BGC-823 gastric cancer cells. Zhonghua Wei Chang Wai Ke Za Zhi 2012;15:1296–300. [article in Chinese]
51. Ferrarotto R, Eckhardt G, Patnaik A, LoRusso P, Faoro L, Heymach JV, et al. A phase I dose-escalation and dose-expansion study of brontictuzumab in subjects with selected solid tumors. Ann Oncol 2018;29: 1561–8.
52. Ferrarotto R, Mitani Y, Diao L, Guijarro I, Wang J, Zweidler-McKay P, et al. Activating NOTCH1 mutations define a distinct subgroup of patients with adenoid cystic carcinoma who have poor prognosis, propensity to bone and liver metastasis, and potential responsiveness to Notch1 inhibitors. J Clin Oncol 2017;35:352–60.
53. Gordon WR, Aster JC. Application and evaluation of anti-Notch antibodies to modulate Notch signaling. Methods Mol Biol 2014;1187: 323–33.
54. Revandkar A, Perciato ML, Toso A, Alajati A, Chen J, Gerber H, et al. Inhibition of Notch pathway arrests PTEN-deficient advanced prostate cancer by triggering p27-driven cellular senescence. Nat Commun 2016;7: 13719.

Published OnlineFirst April 26, 2019; DOI: 10.1158/1535-7163.MCT-18-0804

Molecular Cancer Therapeutics

Loss of Notch1 Activity Inhibits Prostate Cancer Growth and Metastasis and Sensitizes Prostate Cancer Cells to Antiandrogen Therapies

Meghan A. Rice, En-Chi Hsu, Merve Aslan, et al.

Mol Cancer Ther 2019;18:1230-1242. Published OnlineFirst April 26, 2019.